RSC Advances

PAPER

View Article Online
View Journal | View Issue

Cite this: *RSC Adv.*, 2020, **10**, 2952

Three-dimensionally printed polylactic acid/cellulose acetate scaffolds with antimicrobial effect

Mengdi Zuo,[a] Nengyu Pan,[a] Quanjing Liu,[b] Xuehong Ren,[a]* Yu Liu*[b] and Tung-Shi Huang[c]

Received 29th October 2019
Accepted 19th December 2019

DOI: 10.1039/c9ra08916k

rsc.li/rsc-advances

This study aimed to develop novel, biodegradable, antiseptic-loaded and low-cost scaffolds using a direct ink writing (DIW) technique for antibacterial applications. Polylactic acid/cellulose acetate (PLA/CA) mixtures with different composition ratios were prepared, and the effect of CA content on the rheological behaviors of the inks was investigated. The printability of the prepared DIW inks was improved with the addition of the appropriate amount of CA, since the formation of hydrogen bonding 3D network between PLA and CA. As a result, a liquid form ink consisting of majority of PLA and minority of CA which was prepared and printed for the first time through DIW technique. Afterwards, the antimicrobial agent, 1-chloro-2,2,5,5-tetramethyl-4-imidazolidinone (MC) was incorporated into the inks for preventing bacterial infections, which showed excellent stability and effective antibacterial activity against *S. aureus* and *E. coli* O157:H7 in a short time. Owning the ease of fabrication and the biocidal property, our 3D printed scaffolds will have a wide range of potential applications in the field of food packaging, communal facilities, medical equipments, and biomedical materials.

1 Introduction

Additive manufacturing (AM), otherwise known as 3D printing, has been widely considered as a revolutionary manufacturing technology which has promising and significant applications in a broad range of fields including modern devices,[1] sensors,[2] and human tissue and organ engineering.[3] This versatility is related to the specially designed sizes and shapes, along with manufacturing flexibility and efficiency.[4,5] In addition to the tailored architecture, objects can be endowed with the customized functionality accomplished by incorporation of functional compounds into the inks.

Polylactic acid (PLA)-based material has emerged as one of the most promising biocompatible polymers in replacing conventional petroleum-based polymers,[1–5] and has been approved by the Food and Drug Administration (FDA) for a variety of human clinical and ecological applications.[6,7] PLA-based materials have been utilized for fabricating simple two-dimensional to complex three-dimensional scaffolds *via* various techniques, ranging from simple solution casting to advanced 3D printing.[8,9] However, 3D complex manufacturing of PLA parts are mainly carried based on the deposition of successive layers of PLA filaments by fused deposition modelling (FDM) technique in the past literature.[10]

Currently, halogen-based compounds, as antibacterial agents, were adopted and used predominantly to effectively eliminate lethal diseases from infectious pathogens and improve environmental hygiene throughout the world.[11,12] *N*-halamine, a significant subcategory of the halogen antibacterial agents, has drawn significant interests in development of high-performance textiles,[13] biomedical devices,[14] food packaging,[15] stainless steel,[16,17] plastics,[18,19] and paints.[20] The *N*-halamine has comparable antibacterial activities with other biocides such as silver, chitosan and phosphonium salt.[14] More specifically, it further owns the major advantages including broad-spectrum bactericidal properties, high efficiency, long-term physicochemical stability, high durability, regenerability, environmentally friendly, and low manufacturing cost.[21] Therefore, the imidazolidinone-containing *N*-halamine, 1-chloro-2,2,5,5-tetramethyl-4-imidazolidinone (MC) is being introduced into our material design to endow 3D printed devices with antibacterial functionality. However, the high temperature of FDM 3D printing for melting thermoplastic PLA woulvdd cause the negative impacts on the dispersed functional fillers and even could lead to the decomposition of the *N*-halamine in the higher temperature.[22–24] Therefore, other alternative 3D printing approaches should be investigated to avoid the adverse effect on MC.

Lately, direct ink writing (DIW) technique has been studied in 3D bioprinting. In this manufacturing process, the solvent with high vapor pressure can evaporate from the aqueous inks upon exiting from the nozzle and allows a solid part to be built

[a]*Key Laboratory of Eco-textiles of Ministry of Education, School of Textiles and Clothing, Jiangnan University, Wuxi, Jiangsu, 214122, China. E-mail: xhren@jiangnan.edu.cn*

[b]*Key Laboratory of Advanced Food Manufacturing Equipment and Technology, School of Mechanical Engineering, Jiangnan University, Wuxi, Jiangsu, 214122, China. E-mail: yuliu@jiangnan.edu.cn*

[c]*Department of Poultry Science, Auburn University, Auburn 36849, AL, USA*

at ambient temperature. The 3D printing condition of ambient temperature can protect the functional group of the *N*-halamine from decomposition. Recent evidence suggested that the appropriate viscosity and moduli were necessary for the successful extrusion of semi-solid filaments without collapsing. There were no literatures have been reported about the 3D printing of PLA individually by DIW technique. It was reported that cellulose nanofibrils could act as an interfacial stabilizer to enhance the rheological properties of the inks.[25] Huan *et al.* prepared the two-phase and oil-in-water ink, and the internal phase of PLA was stabilized by chitin/cellulose nanofibers.[26] Straightforwardly, DIW of cellulose acetate (CA) to build three-dimensional objects has been investigated. And the results suggested that the feedstock of CA may possess the potential for customized functionalization *via* DIW technique.[27] Nevertheless, the cost associated with obtaining CA might be somehow expensive, although cellulose, as the raw material of CA, is considered the most abundant polymer on the earth. We find that PLA can possess a unique versatility after blending with CA,[28] and the formation of hydrogen bonding 3D network between PLA and CA lead the enhanced interface interaction, which signifies the stable 3D architecture without collapsing.[28,29] Therefore, in this study, we investigate the printability of the different compositions of PLA/CA pasted in DIW, and the effect of CA on the rheological behavior of the inks was discussed. The fabrication process of the antibacterial 3D objects was given in Scheme 1. The work can make a significant contribution to the field of printed antimicrobial 3D complex scaffolds, which have potential application in the field of biomedical materials.

2 Experimental section

2.1 Materials

PLA (4032D) was purchased from NatureWorks LLC (USA). CA (degree of acetylation 38–40%), dichloromethane (DCM), and dimethylformamide (DMF) were provided by Sinopharm Chemical Reagent Co., Ltd (China). MC was obtained from Cangzhou Jincang Chemicals, Ltd (China). All chemicals were used directly without any further purification. The bacterial strains used in this study were *S. aureus* (ATCC 6538) and *E. coli* O157:H7 (ATCC 25922).

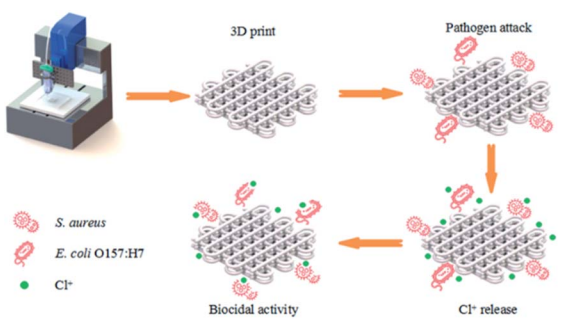

Scheme 1 The manufacturing procedure of 3D printed scaffold and the sterilization process.

2.2 Ink preparation

Liquid inks were prepared by combining commercially available materials of PLA and CA (100/0, 90/10, 70/30, 50/50, 30/70, 10/90, 0/100, w/w) in binary solvent mixture comprising DCM and DMF (7/3, v/v) with mechanical stirring at ambient conditions. To prepare antibacterial PLA/CA scaffolds, MC (1%, 3%, 5%, 7% and 9%, w/w) was added into the inks and the mixture was mixed homogeneously by vortexing. Over the course of several hours, excess DCM was evaporated until a quasi-static shear rate of viscosity was achieved. Under ambient conditions, the high vapor pressure of DCM evaporated rapidly accelerating the drying process of the printed struts and produced self-supporting structures upon extrusion-based printing. The remaining low vapor pressure solvent of DMF imparted enough liquidity and physically smooth transitions between adjacent layers to enable seamless merging of subsequent and adjacent layers. Then, the as-prepared ink mixture was extruded from a microneedle to create architectures. The crucial factor for precision printing was the graded volatility of the solvent.

2.3 Rheological characterization

The prepared inks were analyzed in terms of its rheological behavior in order to evaluate its printability. A rheometer (TA, Discovery HR-2, USA) with a 40 mm flat plate geometry and a gap of 56 μm was used to determine the rheological properties of the inks. Prior to the test, the excessive material outside the plate was scraped off. To determine the viscosity, an analysis was done to record the apparent viscosity as a function of shear rates from 4×10^{-2} to 10^{3} s^{-1}. In the oscillatory measurement, the storage modulus (G') and loss modulus (G'') were recorded as functions of the different stress sweeping from 10^{-1} to 2×10^{4} Pa at a constant frequency of 1 Hz. All measurements were carried out in triplicate and conducted at 25 °C.

2.4 3D direct ink writing process and characterization

A customized DIW 3D printer consists of a computer-controlled three-axis moveable platform, and a pneumatic dispensing module. A conical tip with an inner diameter of 0.25 mm was used. Before 3D printing, the prepared ink mixture was loaded into a luer-lock syringe, followed by sealing with an endcap and centrifuging at 2000 rpm for 5 min to remove any residual bubbles. Then, the syringe barreled with the as-prepared ink being mounted onto the 3D printer. In a typical printing process, the filaments were extruded and printed in parallel with the *X* axis on the silicon substrate with the programmed center-to-center filament spacing and then moved along the *Y* axis to write the filaments, for the formation of a grid structure. The width of the printed filaments and the morphology of the printed scaffolds were assessed with an upright optical microscope (Leica, DVM6 A, Switzerland). Scanning electron microscopy (SEM) images were obtained with a field-emission scanning electron microscope (Hitachi, TM3030, Japan) with an operating voltage of 15 kV. Atomic force microscope (AFM) images were collected in tapping mode on an AFM instrument (Park Systems, XE-100, Korea).

2.5 Chlorine content measurement and antibacterial activity of PLA/CA–MC scaffolds

To assess the chlorine content, scaffolds loaded with MC were immersed in the deionized water at room temperature for 60 min. Potassium iodine (KI) and 0.5% starch solution were added to the resulting solution for iodometric/thiosulfate titration. The contents of oxidative chlorine (Cl^+) on the MC loaded scaffolds were calculated by the equation below:

$$Cl^+ \ (\%) = \frac{N \times V \times 35.45}{2 \times W} \times 100$$

where, Cl^+ (%) is the weight percent of active chlorine content on the scaffold. N and V are the normality (equiv. per L) and volume (L) of the sodium thiosulfate ($Na_2S_2O_3$) titrant, respectively. W is the weight (g) of the titrated sample.

The shaking flask method was employed to investigate the antibacterial property of the scaffolds. The antibacterial activities of the scaffolds (PLA/CA, PLA/CA–MC) were investigated against *S. aureus* and *E. coli* O157:H7. Samples of PLA/CA and PLA/CA–MC scaffolds with the their respective weight of 0.1 g, were dispersed in 10 mL PBS solution with shaking at 200 rpm, and subsequently followed by adding bacterial suspensions (10^6 CFU per sample).

At contact time of 5, 10, and 30 min, 0.5 mL bacterial suspension solution samples were taken out and added into 4.5 mL of PBS and 0.05 N $Na_2S_2O_3$ (8 : 1, v/v) mixed solution. Then, appropriate 10-fold serial dilutions were made, and 100 μL of each dilution were spread on Trypticase® soy agar (TSA) plates in triplicate. The bacterial colonies were recorded after incubation at 37 °C for 24 h and the antimicrobial efficacies were calculated based on the bacterial percentage.

2.6 Storage stability test

The MC-loaded scaffolds were stored in a self-sealed bag under dark environmental condition for a period of 90 days. After the predetermined time of 10, 20, 30, 40, 50, 60, 70, 80 and 90 days, the stabilities of the bound chlorine was analyzed by measuring the remaining Cl^+ content on the scaffolds using the standard iodometric/thiosulfate titration method.

2.7 Evaluation of the release performance

The water release performance test of MC was monitored by a spectrophotometric method.[30] A series of working standard solutions (10, 20, 40, 50, 80, 100 and 125 ppm) were prepared and the respective absorbance values were tested with a UV-vis spectrophotometer (SHIMADZU, UV-2450, Japan) against a deionized water blank at 210 nm, and then the standard MC absorbance concentration calibration curve was made. The scaffolds with the mass of approximately 60 mg were placed in centrifuge tubes containing 10 mL of deionized water for the MC releasing experiments. At predetermined time intervals during the 15 day periods, absorbance of immersion was measured with a UV-vis spectrophotometer and the corresponding concentrations of MC were calculated based on the standard curve.

3 Results and discussion

3.1 Rheological characterization of the ink

DIW was an extrusion-based 3D printing technique, and the ink's capability of flowing smoothly through the nozzle and then retaining the 3D shape were crucial to prevent the printed pattern from collapsing after exiting from the micro-nozzle. The apparent viscosity of the pastes with different fractions (100/0, 90/10, 70/30, 50/50, 30/70, 10/90, 0/100, w/w) were plotted as the function of shear rate and shown in Fig. 1a. All the pastes showed that the apparent viscosity decreased remarkably with the increase of shear rate, indicating that pastes were pseudo-plastic fluids. On the basis of these results, the pastes possessed shear-thinning behaviour, which were suitable for printing.[31]

In addition to viscosity, oscillatory measurements were used to determine the viscoelastic properties of our prepared inks. The stress sweep data are shown in Fig. 1b. It was obviously seen that G'' were always larger than G' under the same concentration of 16.40 wt% for the paste of PLA and the paste of CA. In these conditions, the inks had liquid-like characteristics, namely the inks were unable to maintain the initial configuration when the applied external forces were given to the inks. Surprisingly, G' was larger than G'' when PLA and CA were mixed in the appropriate ratios. The cross appeared in the curves which indicated that G' was equal to G''. Before this point, the G' was higher than the G'' suggesting that the inks predominantly exhibited an elastic behavior at low shear rates. In terms of fluid structure, elastic behavior signified that the intermolecular force was larger than the external force and resulted in a high resistance against deformation of the filament during the printing process. From this point on, G'' was constantly higher than G', indicating that the fluids shifted from "solid-like" to "liquid-like" and the viscous behavior played the dominant effect in the printing process.[32] Under these conditions, the inks could not return to the initial configuration after extrusion from the micro-nozzles. Specifically, it should be noted that the G' value of the ink (PLA:CA = 70 : 30) was distinguished from the G' value of another ink (PLA:CA = 90 : 10). The G' value of the ink (PLA:CA = 70 : 30) was larger in approximately an order of magnitude than that of the ink (PLA:CA = 90 : 10) and was in good agreement with those reported for other colloidal inks designed for DIW technique.[33]

According to previous reports,[28] the existence of hydrogen bonding between the –OH of CA and the –C═O of PLA was attributed to limited extensibility of PLA chains. It was believed here that the increase of magnitude of modulus could be the consequence that the presence of 30% CA restrained the mobility of PLA chains *via* interface interaction of hydrogen bonds. With more CA being added to the blends, the G'' were higher than the G'. It was related to the repulsive forces between the two slightly hydrophobic polymers that further led to the decline of the G' and G'' of the polymeric blend.[28] Therefore, the excessive addition of CA had a negative effect on the printability of the ink. Hence, the results clearly demonstrated that the ink of PLA/CA at 70 : 30 weight ratio was the most desirable material for extrusion.

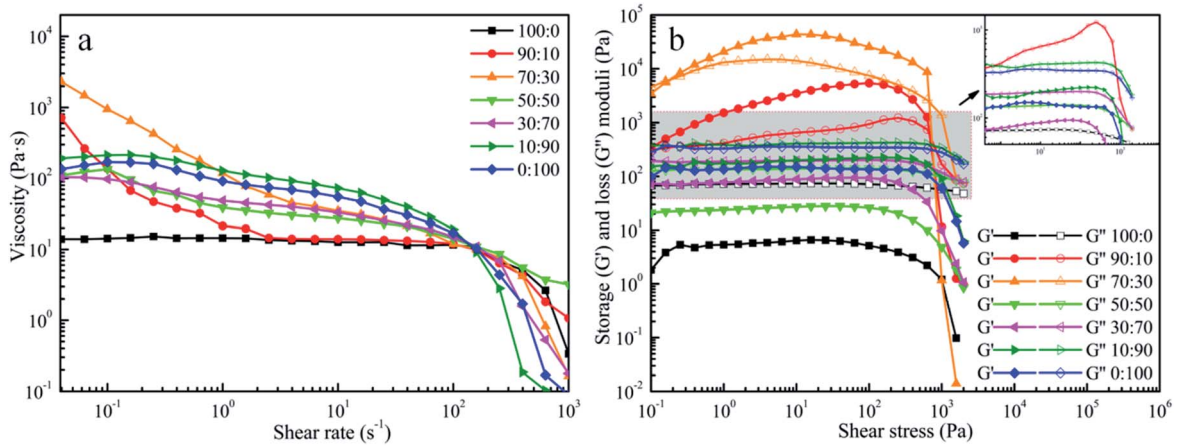

Fig. 1 Rheological properties of (a) the apparent viscosity plot as a function of shear rate in the range of 4×10^{-2} to 10^{3} s^{-1}; and (b) storage and loss moduli as a function of shear stress sweeping from 10^{-1} to 2×10^{4} Pa at a constant frequency of 1 Hz of PLA/CA pastes at different mass ratios (w/w).

3.2 The printing parameters and analysis of tuning chlorine concentration

The filament, as the building block of the printed object, was critical to the quality of the complete structure, and was affected by lair pressure, writing speed and nozzle size. Fig. 2 displays the filament width as functions of the air pressure and the printing speed. As expected, filament width was inversely proportional to printing speed and proportional to air pressure. In general, the faster printing speed could facilitate the print process. However, it might be tough to print with high path accuracy. For example, it could cause discontinuous filaments occasionally. As shown in Fig. 2, it was obvious to observe the ultimate and optimized printing parameters with a print speed of 16 mm s^{-1} and the air pressure of 15 psi to realize the proper and continuous filaments with the width all around 250 μm. Finally, the printed scaffolds were dried at room temperature and peeled off from substrates for further characterization and tests.

The MC and PLA/CA paste were mixed together with different mass ratios of polymers/MC (100/1, 100/3, 100/5, 100/7 and 100/9, w/w). After MC was dispersed uniformly, all inks were printed at room temperature. Fig. 3 shows that the chlorine content in the scaffold with 1% MC was 0.02%, increasing to 0.27% when MC was 5%. However, the chlorine content was closed to the maximum even the concentration of MC was increased. In a short period of time, the MC existing in the inner of filaments released very slow, and then, the active chlorine was hard to be detected. Obviously, the growth rates of chlorine content reached a maximum when the content of MC was 3 wt%. On top of that, 0.13 wt% of Cl^{+} was effective enough to kill bacteria with 3 wt% MC.[34] Therefore, 3 wt% of MC in PLA/CA (7 : 3, w/w) scaffold was selected for the subsequent experiments.

3.3 Morphologies of the scaffolds

The surface morphologies of the PLA/CA and PLA/CA–MC scaffolds were observed by SEM (Fig. 4a and b). It could be

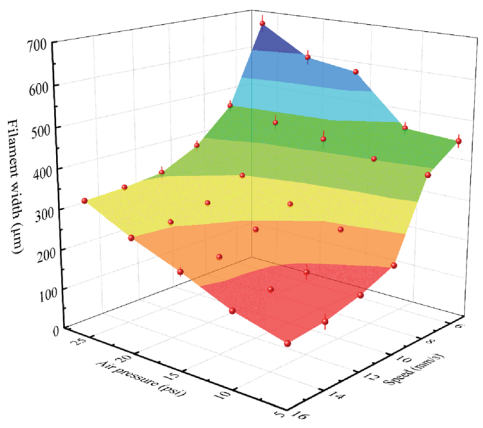

Fig. 2 Filament width of the extruded PLA/CA ink using a nozzle with an inner diameter of 0.25 mm as functions of the air pressure and the printing speed.

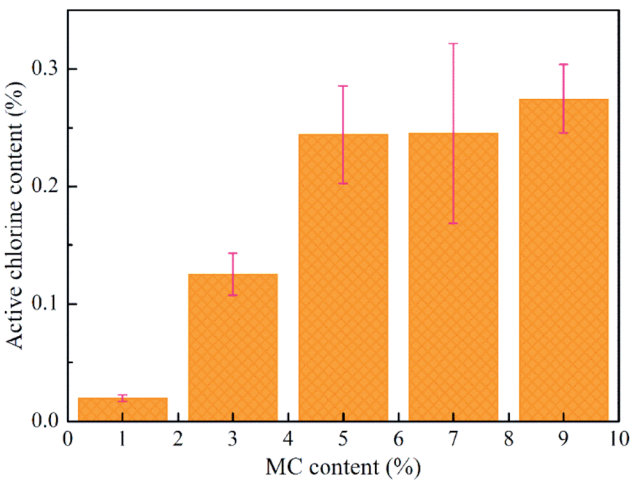

Fig. 3 Relationship of MC content with the chlorine loading of the scaffolds.

clearly seen that some amount of bubbles appeared on the surface of the PLA/CA scaffold, which could be attributed to the evaporation of solvent. After MC loaded on PLA/CA scaffold, as shown in Fig. 4b, the surface appeared cracks and became rougher which might be due to the etching of chlorine.[12] Fig. 4c and d presented the optical images of the microporous mesh-like scaffolds to show the quad-layer structures and the width of the printed filaments which were around 250 μm after the evaporation of solvent. It was tough to achieve such structure through traditional technology of manufacturing. The SEM images of the fracture surfaces were given in Fig. 4e and f. There were few isolated microscale voids indicating the uniformity of the pastes.[27] The tapping-mode of AFM images were performed in Fig. 4g and h. The surface roughness (R_a) of the PLA/CA, and PLA/CA–MC filaments were 20.24 nm and 20.86 nm, respectively, which were in good agreement with the SEM images revealing again the uniformity of the inks. In addition to the grid structure, the DIW technique allowed the manipulation of the different sizes and shapes which were shown by digital image in Fig. 4i. The excellent structural regulation and versatility of the DIW technique, along with convenience, provided additional advantages in manufacturing for various purposes.

3.4 Shelf life stability

Fig. 5 showed the storage stability of MC-loaded scaffolds. After 90 days, the chlorine content of the MC-loaded scaffolds was 0.13 ± 0.01%, which was 100.00% of the initial chlorine level. There was no significant loss of bound chlorine when MC-loaded samples were stored in dark. The results revealed that the MC-added antibacterial materials had excellent storage stability.

3.5 Antibacterial efficacy

The biocidal efficacies of 3D printing scaffolds against *S. aureus* and *E. coli* O157:H7 are shown in Fig. 6. The initial populations of *S. aureus* and *E. coli* O157:H7 were 1.00×10^6 CFU per sample and 1.83×10^6 CFU per sample, respectively. After loaded with MC, the antibacterial activities of the scaffolds against *S. aureus* and *E. coli* O157:H7 were obviously enhanced compared with the PLA/CA scaffolds within 30 min of contact time. The bacterial reductions of *S. aureus* and *E. coli* O157:H7 obviously increased with the extension of contact time, and the bacterial reductions of *S. aureus* and *E. coli* O157:H7 reached to 100.00% within 30 min contact time. The Cl^+ from the N–Cl in the MC compound caused damage to the cell wall through the direct contact with bacteria, which is similar to the inactivation mechanism of oxidative chlorine in hypochlorite (ClO^-).[35] In addition, PLA/CA–MC scaffolds had higher bacterial reductions of *E. coli* O157:H7 than *S. aureus* in 5 min and 10 min contact time. The distinction in inactivating rates was ascribed to the different structures and chemical compositions of their cell walls.[36] Specifically, *E. coli* O157:H7 contains only one thin layer of peptidoglycan, while *S. aureus* possesses multilayers of peptidoglycan in the cell wall, which might provide better protection against antibacterial agent.[37]

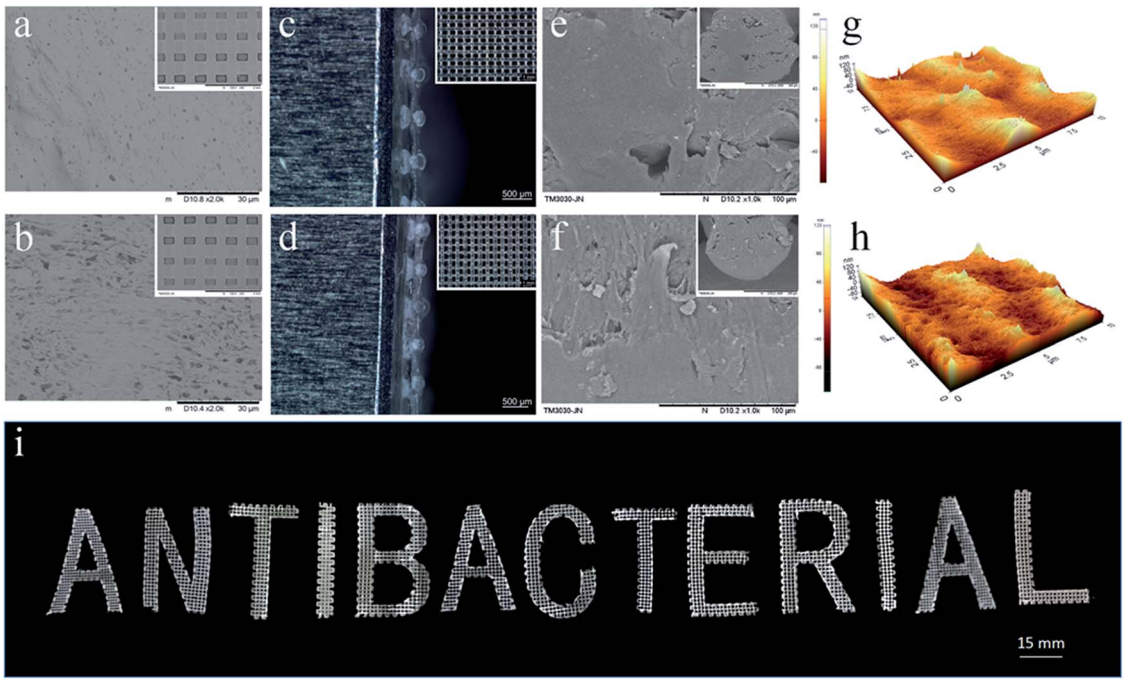

Fig. 4 (a and b) SEM images of the top view of the PLA/CA and PLA/CA–MC scaffolds. Two magnifications are shown with scale bars of 30 μm and 2 mm (insets). (c and d) Optical microscope images of the side view and top view (insets) of the scaffolds with a quad-layer structure. (e and f) Cross section SEM images of the PLA/CA and PLA/CA–MC scaffolds. Two magnifications are shown with scale bars of 100 μm and 200 μm (insets). (g and h) AFM images (10 μm × 10 μm) of the filament surfaces of the PLA/CA, and PLA/CA–MC scaffolds, respectively. (i) Digital image of 3D-printed letters with various shapes and sizes.

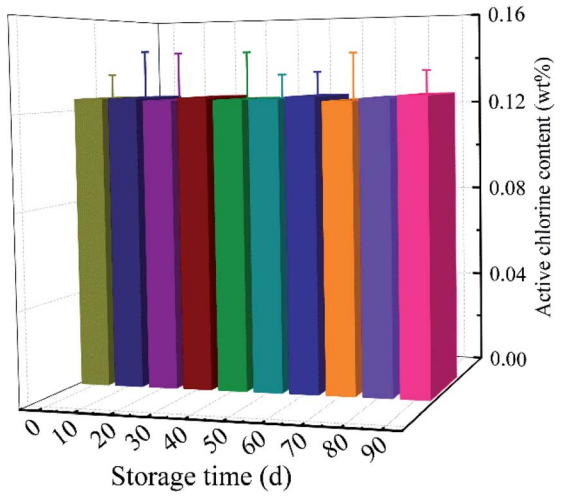

Fig. 5 Storage stability of the active chlorine contents on the PLA/CA–MC scaffolds.

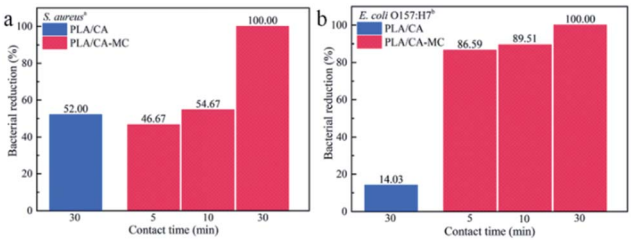

Fig. 6 Antibacterial results of prepared PLA/CA and PLA/CA–MC scaffold against (a) *S. aureus* and (b) *E. coli* O157:H7. [a]Inoculum population was 1.00×10^6 CFU per sample, [b]Inoculum population was 1.83×10^6 CFU per sample.

3.6 Release property of the MC

In order to further study the release profile of MC, the standard curve was created for determining the relationship between the absorption of solutions and the MC concentrations. As depicted in Fig. 7a, the standard curve exhibited fine linear correlation and the linear calibrated equation was listed as follow:

$$y = 0.0065x + 0.0263$$

Based on the linear calibration curve, the relationship between concentration of MC and releasing time was investigated. It can be seen from Fig. 7b that the concentration of MC gradually increased with the extension of time, and reached equilibrium within 10 d. The releasing process could be divided into the early rapid releasing and the subsequent sustained releasing. The data were in agreement with the report from literature.[38] Owing to the sustained releasing property, the antibacterial scaffold was equipped with the prolonged sterilization efficacy upon contacting with bacteria.

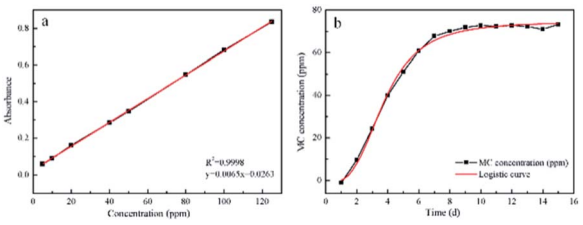

Fig. 7 (a) The standard curve of MC. (b) Released MC levels from PLA/CA–MC scaffolds.

4 Conclusion

Desirable rheological behaviors of the printed inks could be obtained by manipulating the ratios of PLA and CA. The mass ratio of 7 : 3 (PLA:CA) mixture possessed a shear-thinning behavior, which demonstrated an appropriate viscoelastic fluids to ensure efficient flow through nozzles during extrusion and rapid shifting from "liquid-like" to "solid-like" fluid with a sufficient G' for achieving shape retention upon deposition. DIW technique allowed the manipulation of the versatile pore sizes and shapes. The MC loaded PLA/CA scaffolds possessed good antibacterial property, and the bacterial reductions against *S. aureus* and *E. coli* O157:H7 all were 100.00% within 30 min of contact time. In summary, the as-prepared 3D printed antibacterial PLA/CA scaffolds have potential applications in biomedical areas owing to the versatility and convenience in manufacturing by using DIW technique.

Conflicts of interest

There are no conflicts to declare.

Acknowledgements

Authors would like to thank for the research funding from the national first-class discipline program of Light Industry Technology and Engineering (LITE2018-21), the Fundamental Research Funds for the Central Universities (No. JUSRP51722B, No. JUSRP11806), the Project of Jiangsu Science and Technological Innovation Team, and 111 Projects (B17021). Y. L acknowledges the financial support from National Natural Science Foundation of China (Grant No. 51875253) and Jiangsu Key Laboratory of Advanced Food Manufacturing Equipment and Technology (Grant No. FMZ201806).

Notes and references

1 Y. Khane, B. Lahcene and M. Benali, *Biointerface Res. Appl. Chem.*, 2016, **6**, 1104–1111.
2 L. Ribba, L. Tamayo, M. Flores, A. Riveros and S. Goyanes, *J. Appl. Polym. Sci.*, 2019, **136**, 47369.
3 H. Li, C. Zhao, X. Wang, J. Meng and Z. Li, *Adv. Sci.*, 2019, **6**, 1801625.
4 K. Jelonek, A. Zajdel, A. Wilczok, M. Latocha and J. Kasperczyk, *Mater. Lett.*, 2019, **241**, 187–189.
5 J. Z. Wang, M. L. You, Z. Q. Ding and W. B. Ye, *Mater. Sci. Eng., C*, 2019, **97**, 1021–1035.

6 R. M. Rasal, A. V. Janorkar and D. E. Hirt, *Prog. Polym. Sci.*, 2010, **35**, 338–356.
7 N. M. Alves, J. Shi, E. Oramas, J. L. Santos, H. Tomás and J. F. Mano, *J. Biomed. Mater. Res., Part A*, 2010, **91**, 480–488.
8 E. Llorens, *Mater. Sci. Eng., C*, 2015, **50**, 74–84.
9 R. Z. Xing, R. L. Huang, W. Qi, R. X. Su and Z. M. He, *AIChE J.*, 2018, **64**, 3700–3708.
10 B. Kaygusuz and S. Ozerinc, *J. Appl. Polym. Sci.*, 2019, **136**, 48154.
11 N. Y. Pan, Y. Liu, X. H. Ren and T. S. Huang, *Colloids Surf., A*, 2018, **555**, 765–771.
12 N. Y. Pan, Y. Liu, X. Y. Fan, Z. M. Jiang, X. H. Ren and J. Liang, *J. Mater. Sci.*, 2016, **52**, 1–11.
13 Z. Jiang, Y. Liu, R. Li, X. H. Ren and T. S. Huang, *Polym. Adv. Technol.*, 2016, **27**, 460–465.
14 A. Dong, Y. J. Wang, Y. Gao, T. Gao and G. Gao, *Chem. Rev.*, 2017, **117**, 4806–4862.
15 L. J. Bastarrachea, A. Denis-Rohr and J. M. Goddard, *J. Agric. Food Chem.*, 2015, **63**, 4243–4251.
16 B. Demir, R. M. Broughton, T. S. Huang, M. Bozack and S. D. Worley, *Ind. Eng. Chem. Res.*, 2017, **56**, 11773–11781.
17 L. J. Bastarrachea and J. M. Goddard, *J. Appl. Polym. Sci.*, 2012, **127**, 821–831.
18 L. J. Bastarrachea and J. M. Goddard, *J. Agric. Food Chem.*, 2015, **63**, 4243–4251.
19 M. Y. Qiao, T. Ren, T. S. Huang, J. Weese, Y. Liu, X. H. Ren and R. Farag, *RSC Adv.*, 2017, **7**, 1233–1240.
20 H. B. Kocer, I. Cerkez, S. D. Worley, R. M. Broughton and T. S. Huang, *ACS Appl. Mater. Interfaces*, 2011, **3**, 3189–3194.
21 A. Munozbonilla, *Prog. Polym. Sci.*, 2012, **37**, 281–339.
22 X. H. Ren, A. Akdag, C. Y. Zhu, L. Kou, S. D. Worley and T. S. Huang, *J. Biomed. Mater. Res., Part A*, 2010, **91**, 385–390.
23 S. S. Kim and J. Lee, *Cellulose*, 2014, **21**, 4511–4518.
24 W. Lin, A. Liu and Z. Li, *Fibers Polym.*, 2015, **16**, 550–559.
25 S. Q. Huan, R. Ajdary, L. Bai, V. Klar and O. J. Rojas, *Biomacromolecules*, 2019, **20**, 765–771.
26 S. Q. Huan, B. D. Mottos, R. Ajdary, W. C. Xiang, L. Bai and O. Rojas, *Adv. Funct. Mater.*, 2019, **29**, 1902990.
27 S. W. Pattinson and A. J. Hart, *Adv. Mater. Technol.*, 2017, **2**, 1600084.
28 A. H. Ibrahim, A. A. F. Zikry and T. M. Madkour, *Biointerface Res. Appl. Chem.*, 2017, **7**, 2230–2237.
29 Z. Y. Wang, W. L. Gao, Q. Zhang, K. Q. Zheng, J. W. Xu, W. Xu, E. W. Shang, J. Jiang, J. Zhang and Y. Liu, *ACS Appl. Mater. Interfaces*, 2019, **11**, 1344–1352.
30 Y. F. Wang, J. C. Wen, X. H. Ren and Y. Y. Sun, *J. Hazard. Mater.*, 2019, **366**, 651–658.
31 M. J. Regufe, A. F. P. Ferreira, J. M. Loureiro, A. Rodrigues and A. M. Ribeiro, *Microporous Mesoporous Mater.*, 2019, **278**, 403–413.
32 E. Feilden, G. T. Blanca, F. Giuliani, E. Saiz and L. Vandeperre, *J. Eur. Ceram. Soc.*, 2016, **36**, 2525–2533.
33 C. Zhu, T. Y. Han, E. B. Duoss, A. M. Golobic, J. D. Kuntz, C. M. Spadaccini and M. A. Worsley, *Nat. Commun.*, 2015, **6**, 6962.
34 Y. Liu, J. Li, L. Li, S. McFarland, X. H. Ren, O. Acevedo and T. S. Huang, *ACS Appl. Mater. Interfaces*, 2016, **8**, 3516–3523.
35 X. L. Li, Y. Liu, Z. M. Jiang, R. Li, X. H. Ren and T. S. Huang, *Cellulose*, 2015, **22**, 3609–3617.
36 M. J. Osborn, *Annu. Rev. Biochem.*, 1969, **38**, 501–538.
37 J. Tang, Q. Chen, L. G. Xu, S. Zhang, L. Z. Feng, L. Cheng, H. Xu, Z. Liu and R. Peng, *ACS Appl. Mater. Interfaces*, 2013, **5**, 3867–3874.
38 Y. Hui, F. G. Peng, B. W. Wen, X. Y. Xiao, L. Z. Qiao, L. Chong and Z. H. Cheng, *Polym. Chem.*, 2014, **5**, 1965–1975.

